

Pressure-Induced In Situ Construction of P-CO/HNIW Explosive Composites with Excellent Laser Initiation and Detonation Performance

Shanhu Sun, Jinjiang Xu,* Huiyang Gou, Zengming Zhang, Haobin Zhang, Yiling Tan, and Jie Sun*

Cite This: *ACS Appl. Mater. Interfaces* 2021, 13, 20718–20727

Read Online

HPSTAR
1240-2021

ACCESS |



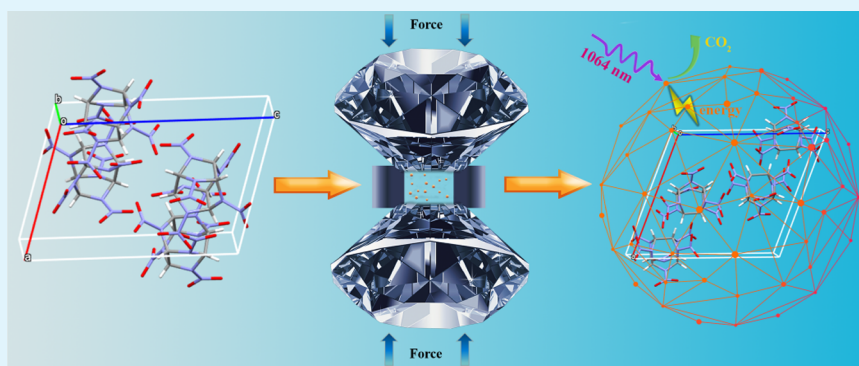
Metrics & More



Article Recommendations



Supporting Information



ABSTRACT: Laser initiation is a popular research topic in the energetic community. Particularly, the direct ignition of secondary explosives by laser ignitors is considered to be an advanced strategy for enhancing safety and promoting the miniaturization of weapons. Here, to improve the laser sensitivity of secondary explosives, P-CO synthesized under high pressure was employed as a coating for HNIW owing to its laser sensitivity and excellent energetic properties. In this operation, HNIW underwent an obvious isostructural phase transition from the ϵ -phase to the γ' -phase in the pressure range of 1.0–4.8 GPa. Subsequently, sub-nanoscale HNIW-based composites were formed when CO in situ polymerized to P-CO on the surfaces of HNIW at 5.1 GPa. This HNIW-based composite could be ignited at a much lower laser power (0.49–0.65 W) compared with pure HNIW (2.75–2.98 W) when excited by an Nd:YAG laser with a wavelength of 1064 nm. Additionally, the DFT calculations demonstrated that the arrangement density between HNIW and P-CO was significantly enhanced as the pressure increased. Thus, the introduction of advanced materials into explosive formulations through high-pressure technology is a novel and feasible strategy for developing multipurpose energetic materials.

KEYWORDS: laser initiation, isostructural phase transition, sub-nanoscale HNIW-based composites, arrangement density, high-pressure technology

1. INTRODUCTION

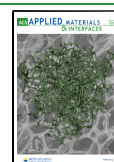
With the growing development of new concept weapons in the military and industry, studies on novel multipurpose energetic materials, such as propellants, explosives, and pyrotechnics, are facing great challenges. In traditional military and commercial blasting, the primary explosives, which are very sensitive to external stimuli, are initiated first. Then, the transfer of the generated shock wave is used to initiate the larger mass secondary explosives such as 1,3,5-trinitro-1,3,5-triazacyclohexane (RDX), 1,3,5,7-tetranitro-1,3,5,7-tetraazacyclooctane (HMX), 2,4,6,8,10,12-hexanitro-2,4,6,8,10,12-hexaazaisowurtzitane (HNIW), and so on. To date, well-known lead-based primary explosives, such as lead azide (LA) and lead styphnate (LS), have been in use for over a century.^{1,2} However, various drawbacks are gradually being discovered. Most importantly, high mechanical sensitivity always leads to many unnecessary

casualties, which means that a controllable trigger entails the risk of unexpected accidents.^{3,4} Additionally, lead-based explosives and their degradable substances pose a great risk to human life and the environment owing to the high toxicity of the heavy metals contained in LA and LS.^{5–8} Hence, the energetic community is currently focusing on the development of novel initiation concepts or green and insensitive primary explosives instead of LA and LS.

Received: February 28, 2021

Accepted: April 14, 2021

Published: April 23, 2021



In recent decades, laser initiation has received widespread attention because it can provide safer, cleaner, and more environmentally efficient ignition systems.^{9–11} However, it is very difficult to synthesize potential high-energy-density materials (HEDMs) with optical sensitive properties because various complex problems related to the energy storage, mechanical sensitivity, and optical properties must be considered in the explosive design. Notably, some high-power laser igniters have been shown to directly ignite the insensitive secondary explosives instead of relying on the sensitive primary explosives. With this strategy, the weapons discarded of the primary explosives can be achieved with enhanced safety, miniaturization, and cost-effectiveness. Considering the low laser absorption of most secondary explosives, some nonenergetic materials such as carbon black,¹² metallic nanoparticles,^{13,14} and chemical dyes¹⁵ have been used to enhance the laser ignition performance of the secondary explosives. For example, Fang et al. mixed 1,1-diamino-2,2-dinitroethene (FOX-7) with approximately 3% (w/w) carbon black powders, which greatly improved the near-infrared (NIR) absorption characteristics.¹² Ji et al. distinctly decreased the initiation power of HNIW by an Nd:YAG laser with a wavelength of 1064 nm by doping with a small amount of aluminum nanoparticles.¹³ However, these nonenergetic materials did not only change the compositions of the explosive formulations but also decreased their energy density. An effective strategy may be to synthesize a laser-sensitive material with excellent detonation performance and dope it with traditional secondary explosives to improve their laser sensitivity.

Currently, some covalently bonded extended phases of specific molecules, which are obtained under high pressure, are attracting a substantial amount of interest owing to their advanced optical, mechanical, and energetic properties.^{16–18} Typically, the triple bond in carbon monoxide (CO) can be broken quite readily under pressure and polymerized under conditions of low pressures and temperatures.^{19,20} One of the resulting products (polymerized CO (P-CO)) has been reported to be an advanced energetic material with disruptive detonation performance owing to its capability of being ignited by moderate NIR irradiation and releasing as much energy as HMX.^{21–23} Coincidentally, polymers have always been considered as ideal candidates for modifying the attributes of energetic materials to endow them with attractive advantages such as high strength, good plasticity, excellent compatibility, and superior corrosion resistance.^{24,25} In terms of the molecular structure of P-CO, the lactone ring and conjugated C=C bond with a high energy content are considered to be the core of P-CO, and these special chemical structures are thought to be capable of strong adsorption with most explosive molecules based on hydrogen bonds and π stacking. If P-CO was employed in traditional explosive formulations, the laser sensitivity of secondary explosives would be significantly improved on the premise of enhancing their safety and detonation performance.

In this study, gaseous CO and HNIW block with a mass ratio of approximately 3:7 were loaded into the pressure device together. Owing to its excellent fluidity, CO was efficiently adsorbed on the surface of HNIW. As the pressure increased, CO in situ polymerized to P-CO and efficiently coated HNIW to form an advanced explosive composite. The experiments and density functional theory (DFT) calculations revealed that this HNIW-based composite has many advantages, such as

high energy storage, sub-nanometer size, and suitable laser sensitivity. Importantly, the high-pressure technique was used for the first time to successfully prepare novel explosive composites.

2. EXPERIMENTAL SECTION

2.1. Materials. The raw HNIW was obtained from the China Academy of Engineering Physics. The CO gas was loaded at the Center for High Pressure Science and Technology Advanced Research.

2.2. Experimental Method. **2.2.1. Preparation of the Explosive Composites of HNIW Coated by P-CO.** The high-pressure experimental conditions were generated using diamond anvil cells (DACs) with 500 μm diameter culets. The specific experimental operations are as follows:

- (a) A stainless steel gasket was preindented to a thickness of 38 μm , and a hole with a diameter of 300 μm was drilled in its center as the sample chamber.
- (b) The HNIW powders were pressed into a flake with a thickness of 25 μm . An HNIW block with a diameter of approximately 285 μm was cut out and then placed at the center of the sample chamber.
- (c) High-purity CO with a pressure of about 22 000 psi (theoretical density of 1.71 g/cm^3) was loaded into the above-mentioned sample chamber. The CO served both as a pressure-transmitting medium (PTM) and reactant.
- (d) When the pressure gradually increased to 5.1 GPa, the CO with a mass ratio of approximately 30% in situ polymerized on the surface of HNIW to form an explosive composite of HNIW coated by P-CO (Figure S1). In this process, the pressure was measured using the ruby fluorescence technique.

2.2.2. Investigation of Unit Cell Parameters of HNIW at Low Temperature. Low-temperature experiments were conducted using a Bruker D8 Advance X-ray diffractometer (XRD) and Cu $K\alpha_1$ radiation ($k = 1.5406 \text{ \AA}$). Liquid nitrogen was used as a cooling substance and the sample temperature was accurately controlled by the TTK 450 thermostat chamber. The diffraction patterns obtained at low temperatures were refined using Topas software.

2.2.3. Laser Ignitability. Laser initiation experiments were conducted using an Nd:YAG solid-state pulsed laser with a wavelength of 1064 nm and power range of 0–20 W. First, all samples were preindented at 5.3 GPa, and the laser spot with a diameter of approximately 15 μm was moved to the center of the samples. Finally, the explosive samples were gradually ignited by improving the laser power.

2.3. Characterization. The Raman spectrum was recorded using an integrated laser Raman system (LABRAM HR, Jobin Yvon) with a stigmatic spectrometer, confocal microscope, and multichannel air-cooled CCD detector. The excitation source was an Ar ion laser ($\lambda_0 = 514.5 \text{ nm}$). Angle-dispersive X-ray diffraction experiments were conducted under pressure at the synchrotron radiation with $\lambda = 0.6199 \text{ \AA}$. The X-ray beam was focused onto a size of approximately $8 \times 11 \mu\text{m}^2$. The diffraction data were recorded using a two-dimensional (2D) imaging plate detector, and the diffraction patterns were integrated and collected using Fit2D software. The morphology was characterized using field emission scanning electron microscopy (FESEM, JSM7900F) equipped with an X-ray energy-dispersive spectroscopy detector (EDS) at the acceleration voltage of 2.5 kV. The X-ray diffraction data were recorded by a Bruker D8 Advance X-ray diffractometer using Cu $K\alpha_1$ radiation ($k = 1.5406 \text{ \AA}$). The operating conditions of the X-ray tube were 40 kV and 40 mA, and a Vantec⁻¹ detector was adopted. The samples were scanned from 5 to 40° with a step width of 0.02° and a scan speed of 0.2 s per step.

2.4. Details of DFT Calculations. Crystal structure calculations were performed using the DFT method with a norm-conserving pseudopotential implemented in the CASTEP program.²⁶ Various density functionals and dispersion-correction schemes were tested in the structural calculations. The generalized gradient approximation (GGA) with the Perdew–Burke–Ernzerhof for Solid (PBEsol),²⁷

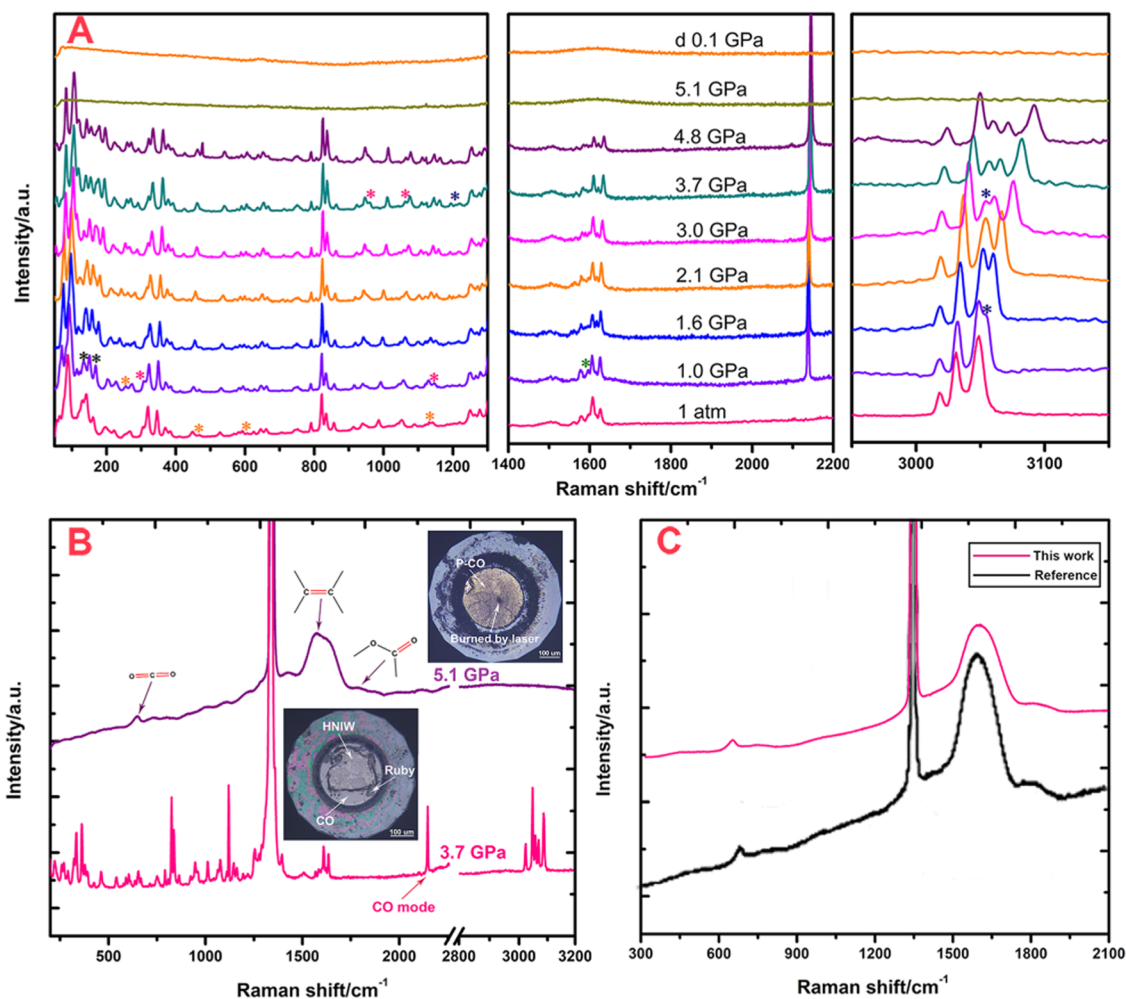


Figure 1. (A) Raman spectrum of ϵ -HNIW crystals with carbon monoxide as the PTM. The obvious changes in this Raman spectrum were marked by asterisks with different colors. (B) Images represented the morphology and Raman spectrum before and after polymerization of CO, respectively. (C) Comparison of the Raman spectrum of P-CO in this work and references.

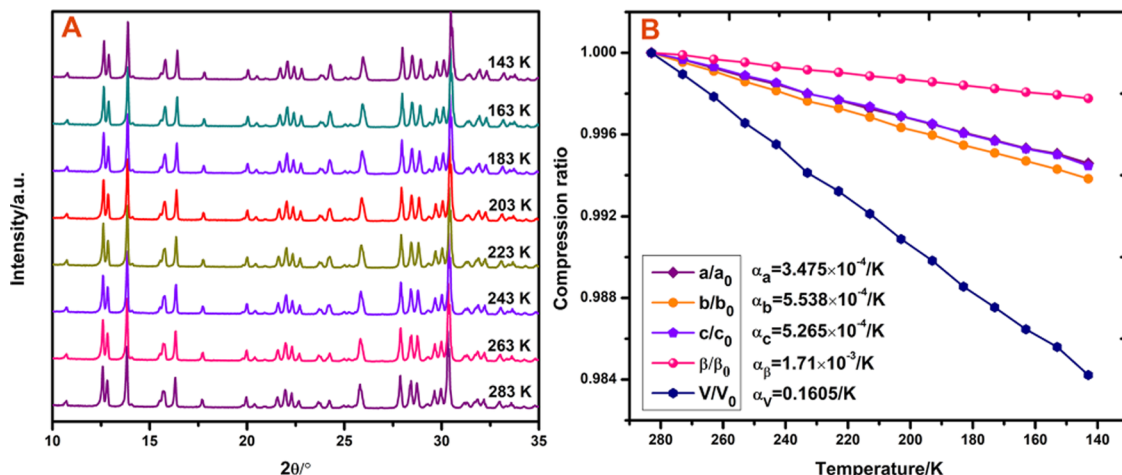


Figure 2. Relationship between the unit cell parameters of ϵ -HNIW and the temperature. (A) In situ XRD patterns of ϵ -HNIW obtained in the temperature range of 283–143 K. (B) Changes in cell parameters of ϵ -HNIW in the temperature range of 283–143 K.

Perdew–Burke–Ernzerhof (PBE),²⁸ and PW91 (Perdew and Wang)²⁹ functionals and local density approximation (LDA)³⁰ of Ceperley and Alder parametrized by Perdew and Zunger (CA-PZ)³¹ were used for structural calculations at 0 K and 101 kPa. To account for the van der Waals (vdW) interactions, various correction methods

such as Tkatchenko and Scheffler (TS), Grimme (D), and Ortman, Bechstedt, and Schmidt (OBS) were employed.³² The norm-conserving pseudopotential was used and the energy cutoff of the plane wave expansion was set to 750 eV. The convergence criteria for geometry optimization were the maximum change in the system

Table 1. Cell Parameters of ϵ -HNIW at 0 K and 101 kPa Obtained by DFT Calculations and Experiments

cell parameters	methods of computation								experimental data (0 K, 101 kPa)
	GGA					LDA			
	CA-PZ D	CA-PZ OBS	PW91 OBS	PW91 TS	PBE TS	PBE D	PBESOL TS	PBESOL D	
a (Å)	8.44	8.50	9.18	9.18	9.04	8.99	8.94	8.76	8.76
b (Å)	11.70	11.73	13.11	13.11	12.83	12.75	12.67	12.33	12.42
c (Å)	12.70	12.73	14.00	14.00	13.68	13.53	13.40	13.15	13.22
V (Å ³)	1215.1	1221.8	1613.5	1615.0	1520.3	1484.9	1446.3	1364.2	1378.7

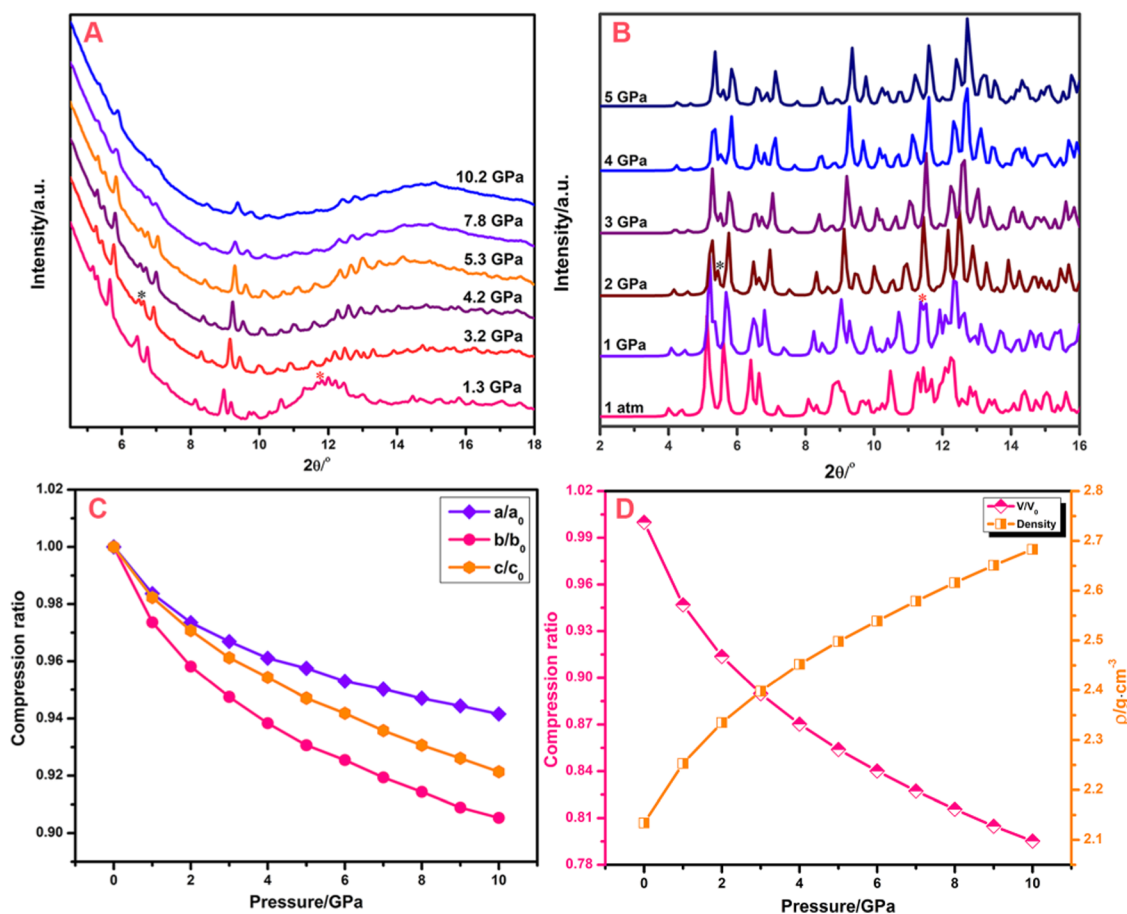


Figure 3. Structural evolution of ϵ -HNIW under pressure was analyzed through experiments and DFT calculations. (A) Synchrotron XRD patterns of ϵ -HNIW obtained under high pressure. (B) Standard XRD patterns simulated through the GGA-PBESOL-D method. (C, D) Changes in the unit cell parameters of ϵ -HNIW with increasing pressure.

energy of 5×10^{-6} eV/atom, maximum force of 0.01 eV/Å, maximum stress of 0.02 GPa, and maximum displacement of 5×10^{-6} Å. For the HNIW crystal, a $3 \times 1 \times 2$ kgrid mesh within the Monkhorst–Pack scheme in the Brillouin zone was employed.

The crystal morphologies of ϵ -HNIW (CCDC: 117779) under different pressures were simulated by the morphology module, and the first three important crystal faces of (011), (110), and (10-1) were selected to calculate the adsorption energy with P-CO. The adsorption energy was calculated using the CASTEP module in the Materials Studio 2019 software.^{33,34} First, GGA-PBESOL-D method was employed to optimize the adsorption models, that is, the P-CO models, models of the three important crystal faces of HNIW, and complex models of the P-CO crystal faces. The default settings were used for all other parameters. Additionally, the adsorption energy was calculated using the following equation

$$E_{\text{ads}} = E_{\text{total}} - E_{\text{P-CO}} - E_{\text{crystal faces}} \quad (1)$$

where E_{total} is the total energy of the complex models of the P-CO crystal faces after the P-CO was adsorbed on the surface of HNIW.

$E_{\text{P-CO}}$ and $E_{\text{crystal face}}$ are the total energy of the P-CO models and crystal faces of the HNIW models, respectively. Accordingly, a negative value of E_{ads} indicates that the adsorption of P-CO on the crystal faces of HNIW is energetically favorable.

The calculation of the excited electronic states of P-CO was carried out using Gaussian 09 suite of programs. The geometric optimization of the structures and frequency analyses were carried out using the B3LYP functional with the 6-31+G* basis set. The optimized P-CO structure was introduced into the energy module, and its excited electronic states were investigated in accordance with the time-dependent theory at the level of B3LYP/6-311.^{35–37}

3. RESULTS AND DISCUSSION

3.1. Characteristics of Explosive Composite of HNIW Coated by P-CO. The in situ Raman spectrum revealed the preparation process of this explosive composite. As shown in Figures 1A and S3, some Raman modes changed significantly as the pressure increased. Most importantly, some modes

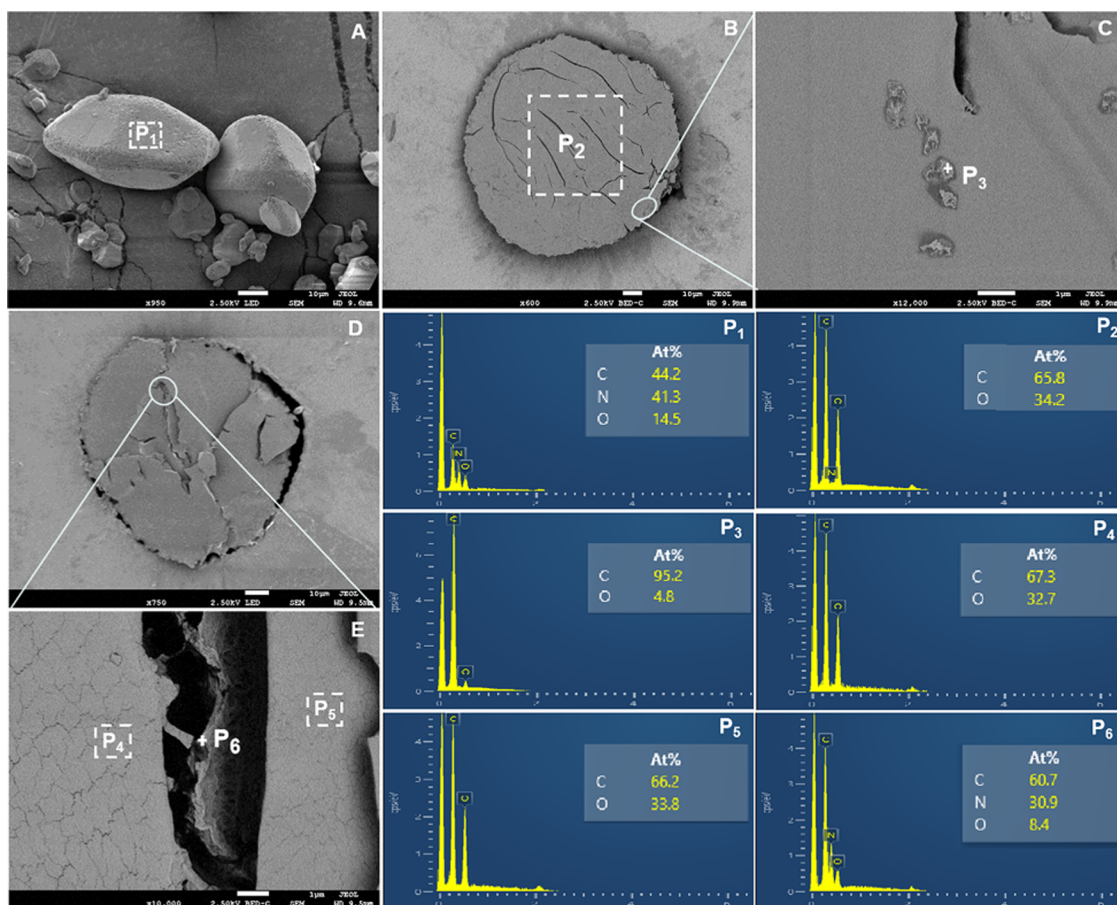


Figure 4. SEM-EDS images. (A) SEM images of raw HNIW. (B) SEM images of an explosive composite including P-CO and HNIW, which recovered under ambient conditions. (C) Enlarged image of image B. (D) SEM images of the explosive composite after its surface was damaged by a scalpel. (E) Enlarged image of image D. (P₁–P₆) EDS spectrum of the marked areas in the corresponding points in the SEM images of A–E.

associated with the C–H stretching and bending vibration exhibited significant changes, particularly in the wavenumber ranges of 3010–3100 and 1200–1250 cm^{-1} , as indicated by the blue asterisks. The C–H bending vibrational peak located at 1257 cm^{-1} split into two separable peaks, while the three C–H stretching vibrational modes located between 3010 and 3100 cm^{-1} split into five modes. Moreover, various single Raman peaks split into separable peaks, such as the CNN bending vibrational peaks (black asterisks), CN/NN stretching vibration peaks (red asterisks), and cage deformation vibration peak (pink asterisks). In contrast, some typical CNN/NCN bending vibration peaks (yellow asterisks) and NO₂ asymmetric stretching vibration peaks (green asterisks) gradually disappeared. According to a study by Sun et al.,³⁸ HNIW exhibited an isostructural phase transition from the ϵ -phase to the γ' -phase, which was initiated at 1.0 GPa and completed at 4.8 GPa in this study. Above approximately 5.1 GPa, the morphology and Raman modes were obviously different, which indicates the occurrence of a chemical reaction. As shown in Figure 1B, the HNIW block and ruby with a clear outline were observed at the center of the gasket hole when the pressure was lower than 5 GPa. The corresponding Raman spectrum comprised the complex modes of HNIW and a characteristic Raman peak of CO located at 2145 cm^{-1} . At 5.1 GPa, the gasket hole was filled with a yellow material, and a novel Raman spectrum contained the symmetric bending mode of CO₂ (650 cm^{-1}). The graphitic C=C stretching mode (1600 cm^{-1}) and C=O stretching mode (1815 cm^{-1}) were detected.

This result is consistent with the conclusions of Evans et al., who reported that these products could be recovered under ambient conditions and comprised five- and six-membered lactone-type rings and conjugated C=C bonds, as shown in Figure 1C.^{19–21}

To understand the structural evolution of ϵ -HNIW under pressure, we carried out in situ synchrotron XRD and DFT calculations. As is well known, in most crystal structure optimization methods, the temperature parameter is set to 0 K by default. To find a more accurate calculation method for optimizing the crystal structure of ϵ -HNIW, its unit cell parameters under 0 K and 101 kPa were successfully derived from the formula describing the relationship between the unit cell parameters and the temperature, which was established through experiments at low temperature as presented in Figure 2 and Tables S1 and S2. Correspondingly, various DFT methods with standard density functions, such as LDA (CA-PZ), GGA (PW91), GGA (PBE), and GGA (PBESOL), were tested for the calculation of the unit cell parameters using the CASTEP module.³² After considering the van der Waals (vdW) interactions, the error of the unit cell parameters calculated using the method of GGA-PBESOL-D was within 1%, compared with the experimental data obtained under at 0 K and 101 kPa, as presented in Table 1.

Based on this accurate calculation method, the crystal structures of ϵ -HNIW under different pressures were optimized, and the changes in the simulated XRD patterns are consistent with those in the experimental synchrotron XRD

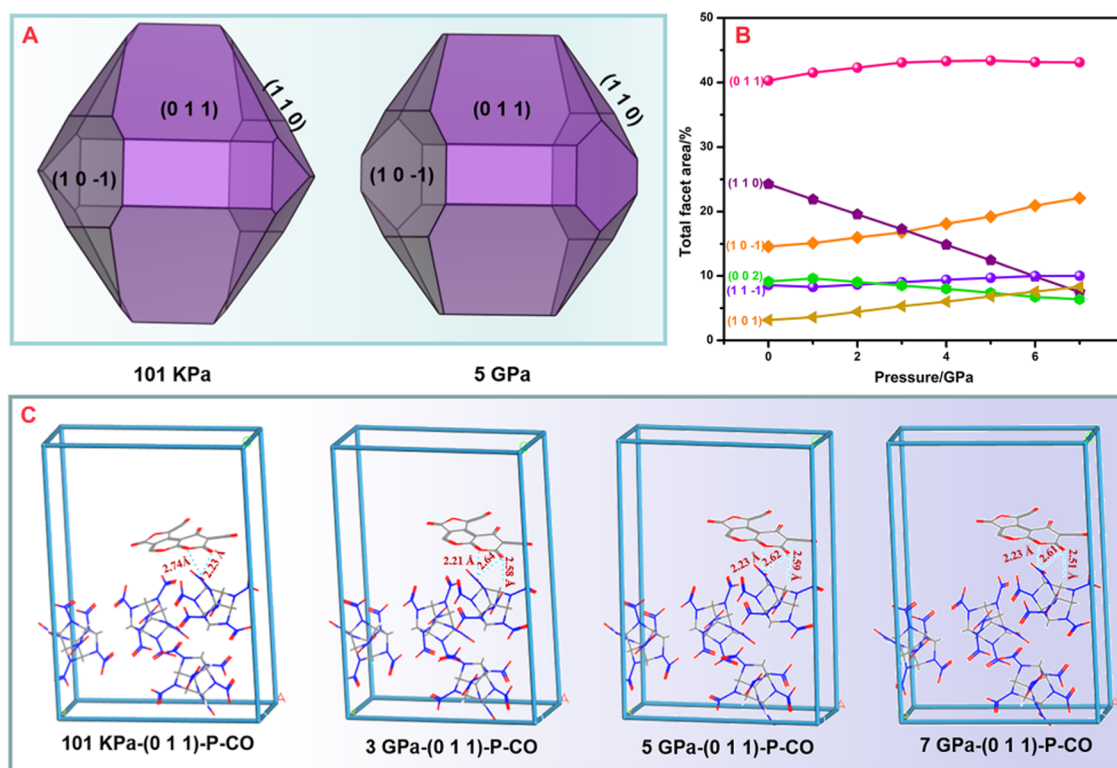


Figure 5. Evolution of adsorption energy between the P-CO and the crystal faces of HNIW with increasing pressure. (A) The morphology modules were simulated by Materials Studio under different pressures. (B) The total facet area of crystal faces of HNIW changed with increasing pressure. (C) The evolution of hydrogen bonds between the crystal face of (011) and P-CO with increasing pressure.

Table 2. Calculated Adsorption Energy between the Important Crystal Faces of HNIW and P-CO under Different Pressures

models	adsorption energy (eV/nm ²)			
	101 kPa	3 GPa	5 GPa	7 GPa
(011)-P-CO	-5.87	-43.78	-74.58	-106.36
(110)-P-CO	-4.19	-35.28	-68.60	-85.56
(10-1)-P-CO	-5.89	-40.88	-69.70	-99.53

patterns, as presented in Figure 3 and Table S3. All diffraction peaks of the synchrotron XRD patterns gradually shifted to smaller d -spacing and various merged or split regions were observed in the pressure range of 1.3–5.3 GPa, as revealed by the experimental synchrotron XRD patterns. These details are more obvious in the simulated XRD patterns, as shown in Figure 3B. Specifically, the d -spacing of the (111) crystal face decreased from 5.56 to 5.46 Å at 0–3 GPa, while that of the (021) crystal face decreased more obviously from 5.55 to 5.27 Å and resulted in two splitting peaks (corresponding to the experimental split peaks located at 6.45°). However, the d -spacing of the (004) crystal face decreased from 3.16 to 3.07 Å, while that of the (202) crystal face was maintained at 3.09 Å, and the approaching d -spacings led to a merged peak (corresponding to the experimental merged peak at 11.65°). Moreover, the relative unit cell parameters of ϵ -HNIW at 10 GPa were $a/a_0 = 94.2\%$, $b/b_0 = 90.5\%$, and $c/c_0 = 92.1\%$. The cell volume of ϵ -HNIW decreased to 79.5%, and the crystal density increased from 2.13 to 2.68 g/cm³, as shown in Figure 3C,D. Therefore, ϵ -HNIW did not exhibit a first-order structural phase transition up to 10 GPa, and the merging or

splitting peaks in the synchrotron XRD patterns were caused by the anisotropy of d -spacing as the pressure increased.

Notably, CO is a very well-known fluid gas with a small molecular volume of approximately 32.4 Å³, and gaseous CO can be uniformly adsorbed on the surface or even at the defects of HNIW under low-pressure conditions. By carrying out SEM and EDS analysis, it was found that the HNIW block was dispersed into many sub-nanoscale composites with clear grain boundaries during the polymerization process of CO to P-CO. As shown in Figures 4 and S2, the raw HNIW exhibited a fusiform morphology and its detected atomic ratios of C, N, and O were 44.2, 41.3, and 14.5%, respectively. After coating with P-CO, only the two elements of C and O with the atomic ratios of 65.8 and 34.2%, respectively, were detected on the surface of this composite. The disappearance of the nitrogen element indicates the absence of HNIW on the surface of this composite. Additionally, a small amount of carbon-rich materials were evenly distributed, which confirms the conclusion whereby P-CO and C were generated in the process of CO disproportionation (Figures 4C and S4).²¹ After damaging the surface of this composite, the HNIW block existed below a thin layer of P-CO (thickness of approximately 100 nm), as indicated by the detection of a nitrogen element belonging to HNIW. The packaging efficiency was significantly higher compared with that of most traditional doping materials, such as graphite³⁹ and graphene oxide.⁴⁰ Therefore, the small special monomers that were in situ polymerized on the surface of the HEDMs provided an effective method for preparing the novel nanoscale explosive composites. As presented in Table S4 based on existing studies, nanoscale energetic materials and mixing with insensitive materials are both effective strategies for enhancing the safety of HEDMs.

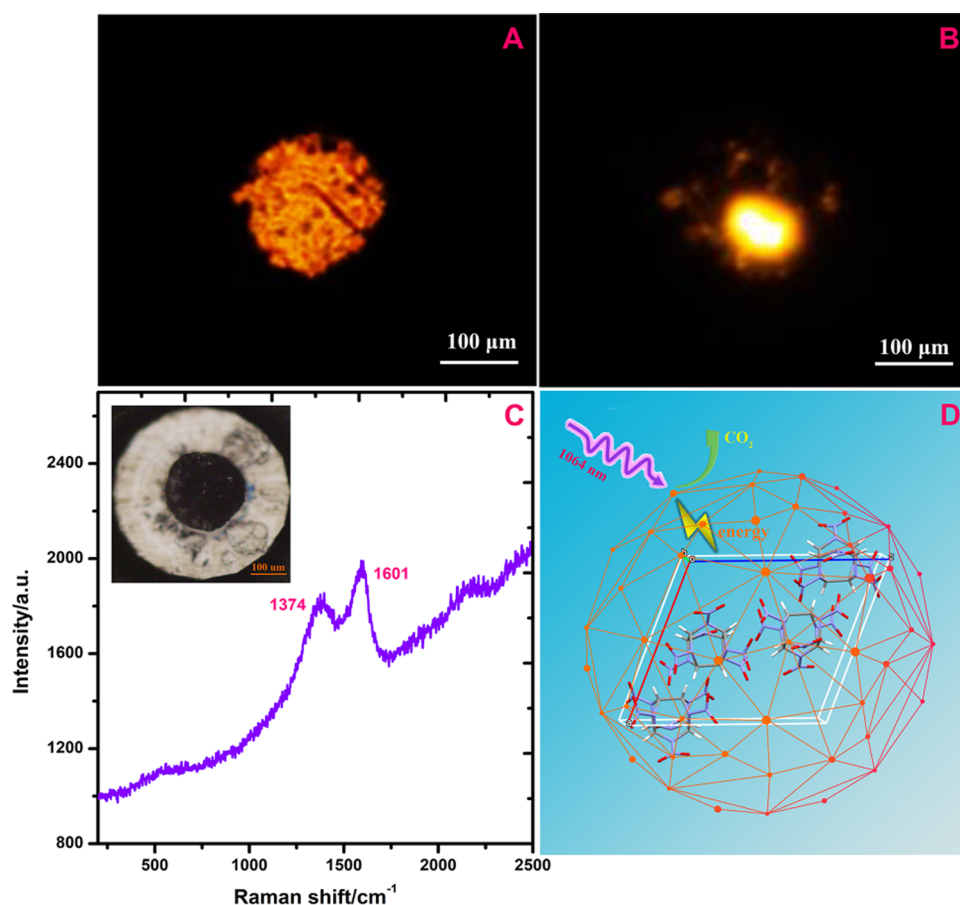


Figure 6. (A) Images of the HNIW-based composite before igniting by laser. (B) Images of the HNIW-based composite after igniting by laser. (C) Raman spectrum of the residue after detonation reaction of the composite. (D) Mechanism of the HNIW-based composite ignited by laser.

Therefore, we believe that the mechanical sensitivity of HNIW can be significantly decreased by coating P-CO with lower energy density on the surface of HNIW to form novel sub-nanoscale explosive composites.

3.2. Evaluation of Detonation Performance. Compared with traditional coatings such as polydopamine⁴¹ and graphene oxide, P-CO is considered an ideal coating for HNIW owing to its excellent detonation performance. Similar to the study by Evans et al. in 2006,²¹ the high energy content of P-CO is considered to rival or exceed that of HMX. Based on the reasonable P-CO structure provided by the above-mentioned study, we compared the energy density of P-CO to that of HMX and HNIW through DFT calculations. Thus, it was found that the energy density of P-CO was 7.36 kJ/g when the P-CO decomposed into graphite and CO₂, which was similar to the energy density of HMX (7.77 kJ/g) but lower than that of HNIW (8.50 kJ/g). The energy density of this HNIW-based composite was approximately 8.16 kJ/g because the composite contained 30% P-CO and 70% HNIW by mass as shown in Table S5. Moreover, in the existing modification operations, the compaction of the two materials is impossible and weakens the energy density of the energetic materials because the detonation pressure largely depends on the square of the density.^{42,43} In this study, it was demonstrated that pressure technology, as an advanced strategy, can overcome the above-mentioned important issues because it cannot only be used to synthesize advanced energetic materials but can also realize dense accumulation between the coating and the explosives. Here, the arrangement density between the interface of HNIW

and P-CO under pressure was evaluated by calculating the adsorption energy. As shown in Figures 5A and S5, the simulation shape of ϵ -HNIW exhibited a typical fusiform morphology with the first three important (*hkl*) crystal faces of (011), (110), and (10-1). As the pressure increased, the different trends exhibited by the total facet area of the crystal faces caused an obvious variation in the crystal morphology. However, the (011), (110), and (10-1) crystal faces still occupied the first three important crystal faces, as presented in Figure 5B and Table S6. The most important adsorption sites were formed between the hydrogen atoms of HNIW and the oxygen atoms from the lactone groups of P-CO. Therefore, the atomic distribution density on the crystal face of HNIW determined the quantity of the adsorption energy at 101 kPa. As presented in Tables 2 and S7 and Figure S6, the (011) crystal face had the strongest adsorption energy of -5.89 eV/nm² with P-CO at 101 kPa because two strong adsorption sites were formed between the hydrogen atoms on the (011) crystal face and the oxygen atoms from the lactone groups of P-CO. Similarly, the roughest crystal face of (10-1) with many atoms perpendicular to the crystal face also had approximate adsorption energy of -5.87 eV/nm² with P-CO, but only one adsorption site was formed between the lowest polarity crystal face of (110) and the lactone groups from P-CO, which resulted in the much weaker adsorption energy of -4.19 eV/nm². As the pressure increased, the adsorption energy was obviously enhanced, mainly owing to the strengthening of the hydrogen bonds and the increase of adsorption sites. For example, at 101 kPa, the distance of the two strong hydrogen

bonds between the (011) crystal face and P-CO was 2.74 and 2.23 Å, respectively. At 7 GPa, these distances were gradually reduced to 2.23 and 2.54 Å, respectively. More importantly, at 3 GPa, a novel strong hydrogen bond began to form between the hydrogen atoms on the crystal face of (011) and the oxygen atoms from the lactone groups, which also played an important role in increasing the adsorption energy. Briefly, this HNIW-based composite was expected to have excellent detonation performance because both HNIW and the P-CO had high energy density and high arrangement density between their interfaces.

3.3. Laser Ignitibility. Traditional primary explosives and initiation methods have been challenged by capricious application environments because most existing ignition mechanisms often rely on extremely high mechanical sensitivity. In recent years, initiation by optical means, such as laser, has drawn a significant amount of attention. However, transparent HNIW crystals have low laser absorption and are difficult to ignite using a low-power laser ignitor. This study demonstrates that P-CO can be excited by NIR irradiation, based on an investigation using time-dependent theory at the level of B3LYP/6-311 with Gaussian 09 (Table S8). After coating using P-CO with a mass ratio of more than 20%, the investigated HNIW-based composite could be ignited at the low power of 0.49–0.65 W under excitation by a laser with a wavelength of 1064 nm, which is significantly lower compared with that of pure HNIW (2.75–2.98 W) as shown in Table S9. The experiment was conducted at 5.3 GPa, and the diameter of the laser spot was approximately 15 μm. The final residue after the detonation reaction was determined to be amorphous carbon, as indicated by the typical D-band at 1374 cm⁻¹ and G-band at 1601 cm⁻¹ in the Raman spectrum shown in Figure 6C. Regarding the ignition mechanism, it is concluded that P-CO could absorb the laser with a wavelength of 1064 nm. The laser with a suitable energy density promoted the decomposition of P-CO into amorphous carbon and CO₂ and released sufficient energy to ignite HNIW, as shown in Figure 6D.

4. CONCLUSIONS

In summary, pressure is an important parameter for regulating thermodynamic stability. Many advanced materials were synthesized under high pressure and have been successfully applied. In this study, a stable high-pressure product with a high energy content, namely, P-CO, was used as a coating for HNIW because it has an excellent performance in terms of high energy density, low mechanical sensitivity, and reasonable laser sensitivity. The in situ polymerization of CO with small volume played an important role in obtaining sub-nanoscale explosive composites, and the packaging efficiency of these composites was significantly higher compared with that of most traditional doping materials. After this operation, this HNIW-based composite could be ignited under much lower laser power (0.49–0.65 W with a wavelength of 1064 nm) compared with pure HNIW. Moreover, through DFT calculations, high-pressure technology was found to be an ideal candidate for preparing dense energetic composites because the arrangement density between the coating and the explosive was significantly enhanced as the pressure increased. Although high-pressure technology is facing enormous challenges with regard to the mass production of various products, we believe that the strategy of synthesizing advanced

explosive composites under high pressure will gradually become widespread.

■ ASSOCIATED CONTENT

Supporting Information

The Supporting Information is available free of charge at <https://pubs.acs.org/doi/10.1021/acsami.1c03856>.

Experimental diagram, theoretical calculations, and characterization data (Raman spectrum, XRD patterns, SEM images, and EDS diagrams) (PDF)

■ AUTHOR INFORMATION

Corresponding Authors

Jinjiang Xu – Institute of Chemical Materials, China Academy of Engineering Physics, Mianyang, Sichuan 621900, China; Email: xujinjiang@caep.cn

Jie Sun – Institute of Chemical Materials, China Academy of Engineering Physics, Mianyang, Sichuan 621900, China; orcid.org/0000-0003-1884-1070; Email: sunjie@caep.cn

Authors

Shanhu Sun – Institute of Chemical Materials, China Academy of Engineering Physics, Mianyang, Sichuan 621900, China; orcid.org/0000-0003-3136-0554

Huiyang Gou – Center for High Pressure Science and Technology Advanced Research, Beijing 100094, China; orcid.org/0000-0002-2612-4314

Zengming Zhang – Department of Physics, University of Science and Technology of China, Hefei, Anhui 230026, China; orcid.org/0000-0001-8245-9955

Haobin Zhang – Institute of Chemical Materials, China Academy of Engineering Physics, Mianyang, Sichuan 621900, China

Yiling Tan – Institute of Chemical Materials, China Academy of Engineering Physics, Mianyang, Sichuan 621900, China

Complete contact information is available at: <https://pubs.acs.org/doi/10.1021/acsami.1c03856>

Notes

The authors declare no competing financial interest.

■ ACKNOWLEDGMENTS

This work was supported by the National Natural Science Foundation of China (Nos. 21805259 and 21975234) and the Defence Technology Projects of China (JCJQ-JJ-418). High-pressure in situ X-ray diffraction was performed at 4W2 HP-Station, Beijing Synchrotron Radiation Facility (BSRF).

■ REFERENCES

- (1) Chen, D.; Yang, H.; Yi, Z.; Xiong, H.; Zhang, L.; Zhu, S.; Cheng, G. C8N26H4: An Environmentally Friendly Primary Explosive with High Heat of Formation. *Angew. Chem., Int. Ed.* **2018**, *130*, 2103–2106.
- (2) Fischer, D.; Klapötke, T. M.; Stierstorfer, J. Potassium 1, 1'-Dinitramino-5, 5'-bistetrazolate: A Primary Explosive with Fast Detonation and High Initiation Power. *Angew. Chem., Int. Ed.* **2014**, *53*, 8172–8175.
- (3) Ma, J.; Tang, J.; Yang, H.; Yi, Z.; Wu, G.; Zhu, S.; Zhang, S.; Li, Y.; Cheng, G. Polynitro-Functionalized Triazolylfuranazone Triaminoguanidine: Novel Green Primary Explosive with Insensitive Nature. *ACS Appl. Mater. Interfaces* **2019**, *11*, 26053–26059.

- (4) Fischer, N.; Joas, M.; Klapotke, T. M.; Stierstorfer, J. Transition Metal Complexes of 3-Amino-1-nitroguanidine as Laser Ignitable Primary Explosives: Structures and Properties. *Inorg. Chem.* **2013**, *52*, 13791–13802.
- (5) Deng, M.; Feng, Y.; Zhang, W.; Qi, X.; Zhang, Q. A Green Metal-free Fused-ring Initiating Substance. *Nat. Commun.* **2019**, *10*, No. 1339.
- (6) Zhang, Q.; Chen, D.; Jing, D.; Fan, G.; He, L.; Li, H.; Wang, W.; Nie, F. Access to Green Primary Explosives via Constructing Coordination Polymers Based on Bis-tetrazole Oxide and Non-lead Metals. *Green Chem.* **2019**, *21*, 1947–1955.
- (7) He, C.; Shreeve, J. M. Potassium 4, 5-Bis(dinitromethyl)-furoxanate: A Green Primary Explosive with a Positive Oxygen Balance. *Angew. Chem., Int. Ed.* **2016**, *55*, 772–775.
- (8) Fischer, D.; Klapotke, T. M.; Stierstorfer, J. 1, 5-Di(nitramino)-tetrazole: High Sensitivity and Superior Explosive Performance. *Angew. Chem., Int. Ed.* **2015**, *54*, 10299–10302.
- (9) Szimhardt, N.; Wurzenberger, M. H. H.; Beringer, A.; Daumann, L. J.; Stierstorfer, J. Coordination Chemistry with 1-Methyl-5Htetrazole: Cocrystallization, Laser-ignition, Lead-free Primary Explosives-One Ligand, Three Goals. *J. Mater. Chem. A* **2017**, *5*, 23753–23765.
- (10) Myers, T. W.; Brown, K. E.; Chavez, D. E.; Scharff, R. J.; Veauthier, J. M. Correlating the Structural, Electronic, and Explosive Sensitivity Properties of CuII Tetrazine Complexes. *Eur. J. Inorg. Chem.* **2016**, *2016*, 3178–3183.
- (11) Fang, X.; Sharma, M.; Stennett, C.; Gill, P. P. Optical Sensitisation of Energetic Crystals with Gold Nanoparticles for Laser Ignition. *Combust. Flame* **2017**, *183*, 15–21.
- (12) Fang, X.; Mcluckie, W. G. Laser Ignitibility of Insensitive Secondary Explosive 1, 1-diamino-2, 2-dinitroethene (FOX-7). *J. Hazard. Mater.* **2015**, *285*, 375–382.
- (13) Ji, X.; Qin, W.; Li, X.; Zheng, S.; Zhou, J.; Xin, Z.; Li, Y.; Wang, L. Initiation of CL-20 Doped with Aluminum Nanoparticles by Using a Laser Pulse through an Optical Fiber. *Propellants, Explos., Pyrotech.* **2018**, *43*, 1210–1214.
- (14) Aduiev, B. P.; Nurmukhametov, D. R.; Furegaa, R. I.; Zvekov, A. A.; Kalenskii, A. V. Effect of Ultrafine Al-C Particle Additives on the PETN Sensitivity to Radiation Exposure. *Combust., Explos. Shock Waves* **2013**, *7*, 453–456.
- (15) Fang, X.; Ahmad, S. R. Laser Ignition of an Optically Sensitized Secondary Explosive by a Diode Laser. *Cent. Eur. J. Energ. Mater.* **2016**, *13*, 103–115.
- (16) Eremets, M. I.; Gavriluk, M. I.; Trojan, I. A.; Dzivenko, D. A.; Boehler, R. Single-bonded Cubic Form of Nitrogen. *Nat. Mater.* **2004**, *3*, 558–563.
- (17) Raza, Z.; Pickard, C. J.; Pinilla, C.; Saitta, A. M. High Energy Density Mixed Polymeric Phase from Carbon Monoxide and Nitrogen. *Phys. Rev. Lett.* **2013**, *111*, No. 235501.
- (18) Iota, V.; Yoo, C. S.; Cynn, H. Quartzlike Carbon Dioxide: An Optically Nonlinear Extended Solid at High Pressures and Temperatures. *Science* **1999**, *283*, 1510–1513.
- (19) Lipp, M. J.; Evans, M. J.; Baer, B. J.; Yoo, C. S. High-energy-density Extended CO Solid. *Nat. Mater.* **2005**, *4*, 211–215.
- (20) Ceppatelli, M.; Serdyukov, A.; Bini, R.; Jodl, H. J. Pressure Induced Reactivity of Solid CO by FTIR Studies. *J. Phys. Chem. B* **2009**, *113*, 6652–6660.
- (21) Evans, W. J.; Lipp, M. J.; Yoo, C. S.; Cynn, H.; Herberg, J. L.; Maxwell, R. S.; Nicol, M. F. Pressure-induced Polymerization of Carbon Monoxide: Disproportionation and Synthesis of an Energetic Lactonic Polymer. *Chem. Mater.* **2006**, *18*, 2520–2531.
- (22) Sun, J.; Klug, D. D.; Pickard, C. J.; Needs, R. J. Controlling the Bonding and Band Gaps of Solid Carbon Monoxide with Pressure. *Phys. Rev. Lett.* **2011**, *106*, No. 145502.
- (23) Xia, K.; Sun, J.; Pickard, C. J.; Klug, D. D.; Needs, R. J. Ground State Structure of High-energy-density Polymeric Carbon Monoxide. *Phys. Rev. B* **2017**, *95*, No. 144102.
- (24) Guan, W.; Wang, Y.; Fischer, C. B.; Fischer, S.; Wang, Z.; Li, J.; Wang, C.; Guo, W.; Xue, Q. Novel Strategy to Improve the Tribological Property of Polymer: In Situ Growing Amorphous Carbon Coating on the Surface. *Appl. Surf. Sci.* **2020**, *505*, No. 144626.
- (25) Love, C. A.; Cook, R. B.; Harvey, T. J.; Dearnley, P. A.; Wood, R. J. K. Diamond Like Carbon Coatings for Potential Application in Biological Implants—a Review. *Tribol. Int.* **2013**, *63*, 141–150.
- (26) Clark, S. J.; Segall, M. D.; Pickard, C. J.; Hasnip, P. J.; Probert, M. J.; Refson, K.; Payne, M. C. First Principles Methods using CASTEP. *Z. Kristallogr. - Cryst. Mater.* **2005**, *220*, 567–570.
- (27) Liu, W.; Liu, W.; Wang, B.; Zhao, Q.; Duan, H.; Chen, X. Molecular-level Insights into the Adsorption of a Hydroxy-containing Tertiary Amine Collector on the Surface of Magnesite Ore. *Powder Technol.* **2019**, *355*, 700–707.
- (28) Perdew, J. P.; Burke, K.; Ernzerhof, M. Generalized Gradient Approximation Made Simple. *Phys. Rev. Lett.* **1996**, *77*, 3865–3868.
- (29) Perdew, J. P.; Wang, Y. Accurate and Simple Analytic Representation of the Electron-Gas Correlation Energy. *Phys. Rev. B* **1992**, *45*, 13244–13249.
- (30) Ceperley, D. M.; Alder, B. J. Ground State of the Electron Gas by a Stochastic Method. *Phys. Rev. Lett.* **1980**, *45*, 566–569.
- (31) Perdew, J. P.; Zunger, A. Self-interaction Correction to Density-Functional Approximations for Many-Electron Systems. *Phys. Rev. B* **1981**, *23*, 5048–5079.
- (32) Dreger, Z. A.; Tao, Y.; Averkiev, B. B.; Gupta, Y. M.; Klapötke, T. M. High Pressure Stability of Energetic Crystal of Dihydroxylammonium 5, 5'-bistetrazole-1, 1'-diolate (TKX-50): Raman Spectroscopy and DFT Calculations. *J. Phys. Chem. B* **2015**, *119*, 6836–6847.
- (33) Sun, H.; Yang, B.; Zhu, Z.; Yin, W.; Sheng, Q.; Hou, Y.; Yao, J. New Insights into Selective-depression Mechanism of Novel Depressant EDTMPS on Magnesite and Quartz Surfaces: Adsorption Mechanism, DFT Calculations, and Adsorption Model. *Miner. Eng.* **2021**, *160*, No. 106660.
- (34) Abraham, B. M. Adsorption Behavior of Explosive Molecules on g-C₃N₄ Nanostructure: a Novel Approach for Sensing Energetic Materials. *J. Phys. Chem. Solids* **2021**, *149*, No. 109777.
- (35) Gao, C.; Li, X.; Qu, Y.; Dai, R.; Wang, Z.; Li, H.; Zhang, Z. Pressure-Dependent Luminescence and Absorption in 3, 3'-Diamino-4, 4'-Azoxyfuran: Secondary Bonding Interaction in Molecular Crystal. *J. Phys. Chem. C* **2019**, *123*, 8731–8739.
- (36) Marenich, A. V.; Cramer, C. J.; Truhlar, D. G. Universal Solvation Model Based on Solute Electron Density and on a Continuum Model of the Solvent Defined by the Bulk Dielectric Constant and Atomic Surface Tensions. *J. Phys. Chem. B* **2009**, *113*, 6378–6396.
- (37) Frisch, M. J.; Trucks, G. W.; Schlegel, H. B.; Scuseria, G. E.; Robb, M. A.; Cheeseman, J. R.; Scalmani, G.; Barone, V.; Mennucci, B.; Petersson, G. A.; et al. *Gaussian 09*; Gaussian, Inc.: Wallingford, CT, 2013.
- (38) Sun, X.; Sui, Z.; Wang, J.; Li, X.; Wang, X.; Dai, R.; Wang, Z.; Huang, S.; Zhang, Z. Phase Transition Routes for ϵ - and γ -CL-20 Crystals under High Pressure up to 60 GPa. *J. Phys. Chem. C* **2020**, *124*, 5061–5068.
- (39) Chen, S.; He, W.; Luo, C.; An, T.; Chen, J.; Yang, Y.; Liu, P.; Yan, Q. Thermal Behavior of Graphene Oxide and its Stabilization Effects on Transition Metal Complexes of Triaminoguanidine. *J. Hazard. Mater.* **2019**, *368*, 404–411.
- (40) Niu, C.; Jin, B.; Peng, R.; Shang, Y.; Liu, Q. Preparation and Characterization of Insensitive HMX/rGO/G Composites via In Situ Reduction of Graphene Oxide. *RSC Adv.* **2017**, *7*, 32275–32281.
- (41) He, W.; Tao, B.; Yang, B.; Yang, G.; Guo, X.; Liu, P.; Yan, Q. Mussel-inspired Polydopamine-directed Crystal Growth of Core-shell n-Al@PDA@CuO Metastable Intermixed Composites. *Chem. Eng. J.* **2019**, *369*, 1093–1101.
- (42) Yan, Q.; Yang, Q.; Zhang, X.; Lyu, J.; He, W.; Huang, S.; Liu, P.; Zhang, C.; Zhang, C.; He, G.; Nie, F. High Density Assembling of Energetic Molecules under Constrain of Defected 2D Materials. *J. Mater. Chem. A* **2019**, *7*, 17806–17814.

(43) Xu, J.; Zheng, S.; Huang, S.; Tian, Y.; Liu, Y.; Zhang, H.; Sun, J. Host-guest Energetic Materials Constructed by Incorporating Oxidizing Gas Molecules into an Organic Lattice Cavity toward Achieving Highly-energetic and Low-sensitivity Performance. *Chem. Commun.* **2019**, *55*, 909–912.